Monthly Notices
of the
ROYAL ASTRONOMICAL SOCIETY

Mon. Not. R. Astron. Soc. **417,** 280–288 (2011) doi:10.1111/j.1365-2966.2011.19209.x

Evidence for a change in the X-ray radiation mechanism in the hard state of Galactic black holes

M. A. Sobolewska,[1,2,3]★ I. E. Papadakis,[2,3] C. Done[4] and J. Malzac[5,6]

[1]*Harvard-Smithsonian Center for Astrophysics, 60 Garden Street, Cambridge, MA 02138, USA*
[2]*Foundation for Research and Technology – Hellas, IESL, Voutes, 71110 Heraklion, Crete, Greece*
[3]*University of Crete, Dept of Physics and Institute of Theoretical and Computational Physics, Voutes, 71003 Heraklion, Crete, Greece*
[4]*University of Durham, Department of Physics, South Road, Durham, DH1 3LE*
[5]*Université de Toulouse; UPS-OMP; IRAP; Toulouse, France*
[6]*CNRS; IRAP; 9 Ave colonel Roche, BP 44346, F-31028 Toulouse cedex 4, France*

Accepted 2011 June 7. Received 2011 June 7; in original form 2011 February 03

ABSTRACT

We present results on the spectral variability of two Galactic black hole X-ray binaries, GRO J1655–40 and GX 339–4, in the hard state. We confirm a transition in behaviour of the photon index with luminosity, such that the well-known decrease in X-ray photon index with decreasing luminosity only continues down to $L_{\rm bol} \sim 0.01 L_{\rm E}$. Below this point, the photon index increases again. For Comptonization models, this implies that the ratio of the Compton luminosity to seed photon luminosity, $\ell_{\rm h}/\ell_{\rm s}$, changes with bolometric luminosity, consistent with a scenario where seed photons change from cyclo-synchrotron at the lowest luminosities to those from a truncated disc. Alternatively, the transition could mark the point below which the non-thermal jet starts to dominate, or where reprocessed photons replace the viscous photons in an outflowing corona model.

Key words: accretion, accretion discs – black hole physics – X-rays: binaries.

1 INTRODUCTION

Galactic black hole binaries (GBHs) are strong sources of X-ray radiation. This radiation can be decomposed into two main components: soft thermal radiation, originating in an accretion disc, and hard power-law-like emission, probably originating in the process of Comptonization of the disc photons by hot electrons located in the so-called corona (see reviews by Remillard & McClintock 2006; Done, Gierliński & Kubota 2007; and references therein). The disc and corona contribute at different levels to the total spectrum. Consequently, a number of different GBH spectral shapes have been observed and these have been classified into two main spectral states. In the soft state, the hot disc dominates the spectrum up to a few keV and it is accompanied by a weak power-law tail with a soft photon index, $\Gamma > 2$. In the hard state, the disc is much cooler and the total X-ray band is dominated by the radiation of the corona with typically a hard photon index, $\Gamma < 2$.

The physical origin of the transitions between the spectral states is not clear yet. Nevertheless, phenomenologically, the evolution of the X-ray spectral shape within a given state and during the transition from one state to another is relatively well understood. The GBHs in outburst track the same, continuous q-shaped pattern in the so-called hardness–intensity diagram (HID; e.g. Fender, Belloni & Gallo 2004; Dunn et al. 2008). From this diagram, it follows that initially the X-ray spectra of GBHs are dominated by a hard colour and their intensity is low; the sources are in a hard state and reside in the bottom/right corner of the HID. With time, the intensity increases but the spectra remain dominated by the hard colour; the sources move upwards in the diagram. At some point, a further increase in intensity results in the decrease of hardness, and the sources move toward the top/left part of the HID. Eventually, a transition to a soft state takes place, resulting in populating the top/left section of the HID. Towards the decay of the outburst, the intensity decreases and a transition back to a hard state is observed. The soft-to-hard state transition occurs typically at lower intensity than the hard-to-soft state transition at the beginning of the outburst (e.g. Gierliński & Newton 2006), which leads to a hysteresis pattern in the HID. A theoretical explanation of the hysteresis includes the effects of different sources of coronal irradiation in the hard and soft states (Meyer-Hofmeister, Liu & Meyer 2005, 2009), and in the most extreme cases a non-steady state behaviour, when the mass accretion rate changes by several orders of magnitude over a period of week, or a shorter period (Gladstone, Done & Gierliński 2007). The X-ray spectral evolution in the HID correlates with the X-ray variability properties (Belloni et al. 2005) and with properties of the radio emission from a jet (Fender et al. 2004).

In the HID, an increase in intensity is associated with an increase in the mass accretion rate, while a decrease in hardness corresponds to a softening of the X-ray photon index. A number of scenarios

★E-mail: msobolewska@cfa.harvard.edu

have been presented to explain the spectral evolution of GBHs, that is, the spectral softening (hardening) with increasing (decreasing) mass accretion rate (e.g. see reviews in Remillard & McClintock 2006; Done et al. 2007). One of the scenarios is that of the truncated accretion disc (e.g. Esin, McClintock & Narayan 1997). In this model, at low mass accretion rates, the standard accretion disc in the hard state is truncated far away from a black hole, and a hot inner flow is formed close to the black hole. In such a geometry, few disc photons can be intercepted by the hot flow, and the resulting spectra have a hard photon index, characteristic of the hard state. As the mass accretion rate increases, the inner radius of the disc moves closer to the black hole, resulting in an increased cooling of the electrons. Consequently, the spectrum softens and the source evolves to a soft state. The soft-state spectra seem to be well understood in terms of the multicolour disc blackbody emission from an untruncated (extending to the innermost stable circular orbit) disc accompanied by a weak Comptonized hard tail. Alternative hard-state models not involving a truncated disc have been proposed (see Done et al. 2007 for the strengths and weaknesses of each model). These include, for example, a patchy outflowing corona above a disc extending to the last stable orbit (Beloborodov 1999a; Malzac, Beloborodov & Poutanen 2001) and the jet origin of the hard X-rays (Markoff, Falcke & Fender 2001).

However, several recent studies have shown that in the hard state at very low mass accretion rates, below a few per cent of the Eddington rate, the spectra of GBHs begin to soften again while the luminosity decreases (e.g. Ebisawa et al. 1994; Revnivtsev, Trudolyubov & Borozdin 2000; Corbel et al. 2004; Jonker et al. 2004; Kalemci et al. 2005; Wu & Gu 2008; Dunn et al. 2010). Interestingly, a similar spectral evolution with luminosity has also been reported in the case of active galactic nuclei. Above a certain luminosity, the photon index softens with increasing luminosity (e.g. Porquet et al. 2004; Shemmer et al. 2006; Saez et al. 2008; Sobolewska & Papadakis 2009), but at low accretion rates the opposite trend is observed – the photon index hardens while the luminosity increases (Constantin et al. 2009; Gu & Cao 2009), just as in GBHs.

As mentioned, it is generally believed that the hard power-law-like X-rays are produced from Compton upscatter of soft disc photons by energetic electrons in a hot corona located close to the black hole. The high-energy cut-offs observed in the hard-state spectra suggest that the population of electrons is thermal (e.g. Gierliński et al. 1999; Rodriguez, Corbel & Tomsick 2003; Joinet, Kalemci & Senziani 2008; Miyakawa et al. 2008; Motta, Belloni & Homan 2009). Within this framework, the main parameter that determines the spectral shape of the intrinsic hard X-ray continuum in accreting sources is the ratio of heating-to-cooling compactnesses, ℓ_h/ℓ_s, where compactness is defined as a dimensionless luminosity:

$$\ell = \frac{L}{R}\frac{\sigma_T}{m_e c^3}. \quad (1)$$

Here, L is the luminosity of a spherical region of radius R and σ_T is the Thomson cross-section.

In this paper, we study how the compactness ratio, ℓ_h/ℓ_s, evolves with GBH luminosity in the hard state. We consider the rising and decaying parts of the outbursts of two confirmed black hole binaries, when their luminosity is less than ∼0.1–0.3 of their Eddington limit. We fitted their spectra with a disc blackbody component (to account for their disc emission in soft X-rays) and the EQPAIR model of Coppi (1999) to determine ℓ_h/ℓ_s. Because this parameter is mainly determined by the disc/corona geometry, our aim is to infer and constrain the evolution of the source geometry in the hard state, and to investigate which of the current theoretical models are consistent with our results.

2 DATA SELECTION

In this work, we re-analyse all the archival *Rossi X-ray Timing Explorer* (*RXTE*) observations of GRO J1655–40 and GX 339–4, available up to 2007. Both sources are well-studied systems, containing a dynamically confirmed black hole primary (see references in Table 1). The GRO J1655–40 selected data cover in great detail the period of its 2005 outburst. In addition, the mass and distance to GRO J1655–40 are relatively well constrained (Table 1; see Foellmi 2009, and Section 4.3), which allows for accurate conversion of the observed fluxes into the Eddington luminosity ratios. The GX 339–4 selected data extend over a time-scale of several years. These cover reasonably well its 2002/2003 and 2004/2005 outbursts (o2 and o3, respectively) and include observations taken in the period of 1996–1999 (o1). Even though the mass and distance constraints of GX 339–4 are not as tight as those of GRO J1655–40, we have chosen this system for our study because of the large number of hard-state observations displayed in its multiple outbursts. Both sources follow a well-known q-shaped pattern in the colour–intensity diagram (e.g. Dunn et al. 2010), which means that their X-ray spectral properties are typical of GBHs. Hence, we believe that the data we have selected are representative of the GBH behaviour during the luminosity rising and decaying phases of an outburst.

We extracted archival Standard 2 spectra for detector 2, top layer, in the 3–20 keV band and High-Energy X-ray Timing Experiment

Table 1. Log of the *RXTE* observations. The columns show the following: (1) the name of the source; (2–4) the year and the dates of the first/last observations we studied; (5) the hydrogen column density used in the spectral fits; (6–8) the distance (the uncertainty on the distance from the literature), inclination and black hole mass of the systems; (9) the number of analysed hard-state observations. The references for the entries in columns (5–8) are as follows: [1] Done & Gierliński (2003); [2] Orosz & Bailyn (1997); [3] Remillard & McClintock (2006); [4] Hynes et al. (2004); [5] Zdziarski et al. (2004); [6] Muñoz-Darias, Casares & Martínez-Pais (2008); [7] Kolehmainen & Done (2010).

Source	Year	Start MJD[a]	End MJD[a]	N_H $\times 10^{22}$ cm^{-2}	D kpc	i	M M$_\odot$	Number
(1)	(2)	(3)	(4)	(5)	(6)	(7)	(8)	(9)
GRO J1655–40	2005	53423	53673	0.8 [1]	3.2 (3.0–3.4) [1]	70° [2]	6.3 (6.0–6.6) [3]	94
GX 339–4	1996–1999 (o1)	50291	51441	0.6 [1]	10 (6–15) [4–6]	30° [b]	10 (6.2–15) [6, 7]	224
	2002/2003 (o2)	52367	52774					
	2004/2005 (o3)	53044	53537					

[a]Modified Julian Date, MJD = JD – 240 0000.5.
[b]Because the inclination to GX 339–4 is unknown, we assume 30°.

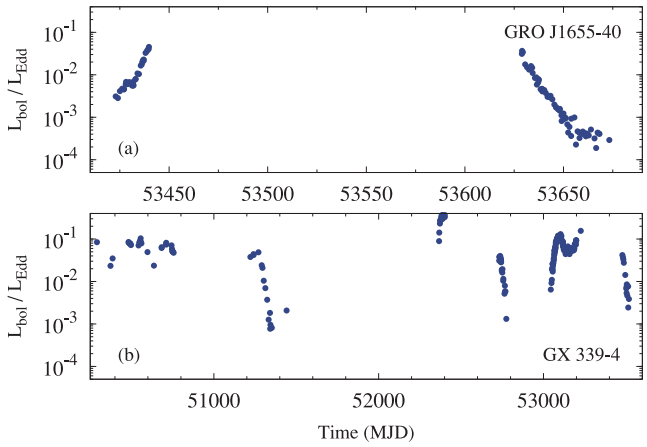

Figure 1. Hard-state light curves of (a) GRO J1655–40 and (b) GX 339–4 (see, for example, Done et al. 2007 for complete light curves). Bolometric luminosities in Eddington units have been calculated based on the best-fitting models of Sobolewska et al. (2011, GRO J1655–40) and model 2 in this paper (GX 339–4) extrapolated to the 0.01–1000 keV band.

(HEXTE) spectra from both detectors in the 20–200 keV band. The details on data reduction are given in Sobolewska, Gierliński & Siemiginowska (2009). Standard methods were used to subtract the background, to create response matrices and to deal with systematic errors. We obtained one spectrum per pointed observation.

Of all the available *RXTE* observations, we chose to study the data when the source's high-energy spectrum has a photon index $\Gamma < 2$, as found from the Proportional Counter Array (PCA) + HEXTE 3–200 keV model fits, including the thermal Comptonization component (Sobolewska et al. 2009). Fig. 1 shows the X-ray luminosity in Eddington units plotted as a function of time, for the selected *RXTE* observations of the two sources. The rising/decaying phases of the outbursts can be clearly seen. In all cases, the source luminosity was lower than 10 per cent of the Eddington limit for GRO J1655–40, and 30 per cent for GX 339–4. Consequently, during these observations both systems should mainly be in their hard state. Luminosity estimates are based on model 2, which we describe in the next section. In total, we studied 94 and 224 hard-state observations of GRO J1655–40 and GX 339–4, respectively.

In Table 1, we list the time period covered by the selected data, the hydrogen column density used in the spectral fits, the physical properties (i.e. distance, inclination and black hole mass) that we adapted in this work and the number of hard-state observations that we studied. The distance to GRO J1655–40, and its mass are known quite accurately (but see Foellmi 2009). However, the estimates for GX 339–4 suffer from significant uncertainties. So, in this work we adopted the canonical values (for GBHs) of $10\,M_{\odot}$ and 10 kpc for this source.

3 SPECTRAL MODELLING

The process of Comptonization of the soft disc photons in the hot corona is widely accepted as the mechanism responsible for the bulk of the power-law-like continuum in the X-ray spectra of accreting objects. We considered two different models to fit the 3–200 keV band spectra of our two sources. We included a multicolour disc blackbody (DISKBB in XSPEC) in both of them to account for the disc emission. As for the power-law continuum, we used two different Comptonization models: the THCOMP thermal Comptonization routine of Zdziarski, Johnson & Magdziarz (1996) and the EQPAIR code of Coppi (1999). In both models, we fixed the temperature of the soft disc photons at $kT_{bb} = 0.4$ keV because the *RXTE* low-energy bandpass does not provide enough coverage to measure properly the temperature of the cool hard-state discs. We modelled the spectra using XSPEC version 11.3.2 (Arnaud 1996).

3.1 Estimating the photon index

Sobolewska et al. (2009) modelled the 3–200 keV PCA/HEXTE data of several GBHs. They used a model consisting of DISKBB, THCOMP, a Gaussian line profile to model iron Kα features, and a smeared edge (SMEDGE) to account for iron Kα absorption. The complete model was described in XSPEC as CONSTANT*WABS*SMEDGE*(GAUSSIAN + DISKBB + THCOMP), hereafter model 1. The N_{H} for the absorption component WABS was kept fixed to the Galactic column density listed in Table 1. A constant component was added to account for differences between the PCA and HEXTE normalizations (the constant was fixed at 1 for PCA and was left free to vary for HEXTE). We used the results of Sobolewska et al. (2009) to study the evolution of the photon index in GRO J1655–40 and GX 339–4.

3.2 Estimating the heating-to-cooling compactness ratio

Sobolewska, Siemiginowska & Gierliński (2011) modelled the hard-state GRO J1655–40 observations of the 2005 outburst replacing the THCOMP model with EQPAIR, a hybrid thermal/non-thermal Comptonization model (Coppi 1999; Gierliński et al. 1999). The main parameter determining the spectral shape in the EQPAIR model is the ratio between the compactness of seed photons, ℓ_{s}, and hot electrons, ℓ_{h}. This ratio, ℓ_{h}/ℓ_{s}, defines the spectral shape of the Comptonized continuum. It is a physical parameter (as opposed to the photon index in model 1) and it depends mostly on the geometry of the accretion flow. Typically, the hard-state spectra are characterized by $\ell_{h}/\ell_{s} \gg 1$, the soft-state spectra by $\ell_{h}/\ell_{s} \ll 1$ and the very high/intermediate state spectra by $\ell_{h}/\ell_{s} \sim 1$. The complete model was defined in XSPEC as CONSTANT*WABS(DISKBB+EQPAIR), hereafter model 2, where CONSTANT and WABS are defined as in model 1.

As described in Sobolewska et al. (2011), eight of 94 hard-state observations showed residuals around 6–7 keV, reminiscent of an iron line. Thus, the LAOR relativistic line model (Laor 1991) was included to improve these fits (EQPAIR does not account for the iron line emission). With this addition, model 2 fits to all 94 hard-state data sets of GRO J1655–40 resulted in a null hypothesis probability higher than 0.05.

We applied the same model to the selected hard-state observations of GX 339–4. We found that 48 of 224 data sets required an addition of the iron line, and again we added the LAOR component to model 2. Following this, the model provided a good fit (with a null hypothesis probability higher than 0.05) to 220 of the 224 data sets. We therefore conclude that model 2 is a good description of the hard-state spectra of this source as well.

We use the results of Sobolewska et al. (2011) for GRO J1655–40 and our results for GX 339–4 to study the hard-state evolution of ℓ_{h}/ℓ_{s}.

3.3 Estimating the bolometric luminosity

The spectra we have studied are characterized by a photon index lower than ~2. We assume that they originate in a process of thermal Comptonization, and so they peak in the EF_{E} representation at energies of the order of the temperature of the thermal electron. Indeed,

many of our spectra show a rollover at energies of the order of 100 keV. In order to estimate the total X-ray flux, and to ensure that we do not neglect any energy radiated above 100 keV, we extrapolated the best-fitting model 2 spectra and we estimated the flux in the 0.01–1000 keV band, $F_{0.01-1000}$. Because the majority of energy in GBHs is radiated in the X-ray band, we considered $F_{0.01-1000}$ to be representative of the bolometric flux. Assuming isotropic emission, we define bolometric luminosity as $L_{\rm bol} = 4\pi D^2 F_{0.01-1000}$, for a black hole located at a distance D. We study the spectral evolution of our sources as a function of bolometric luminosity in Eddington units, $L_{\rm bol}/L_{\rm E}$, where $L_{\rm E} = 1.3 \times 10^{38}(M/{\rm M}_{\odot})$ erg s^{-1} for a black hole of mass M.

4 SPECTRAL EVOLUTION IN THE HARD STATE

4.1 X-ray colour evolution

We first considered the evolution of the X-ray colour with source accretion rate in order to study the spectral variability of the two sources in a model-independent way, without any a priori assumption about the shape of the X-ray continuum. Following Belloni et al. (2005), we defined the X-ray colour as the ratio of the observed count rates in the hard (i.e. 6.3–10.5 keV) and soft (i.e. 3.8–6.3 keV) X-ray energy bands. Our results are shown in Figs 2(a) and (d). Note that, traditionally, this type of plot shows a count rate as a function of X-ray colour. However, we chose to plot the Eddington luminosity ratio to help with a more straightforward comparison of Figs 2(a) and (d) with the following plots in this paper.

The figures clearly show that the X-ray spectra of GRO J1655–40 and GX 339–4 vary with luminosity during the hard state. The X-ray colour follows a well-defined pattern, which is similar in both sources. It first increases (i.e. the hard X-rays become more dominant) with increasing luminosity until $L_{\rm bol}/L_{\rm E}$ reaches the value of ∼1–3 per cent, above which the colour decreases. This value obviously depends on the adopted distance and black hole mass estimates for each source. However, the inferred spectral evolution with luminosity cannot be attributed to any specific model assumptions because the colour was calculated using the observed count rates. We indicate the rising and decaying phases of the outbursts with different symbols; note the hysteresis pattern in both sources.

4.2 Photon index evolution

Although the X-ray colour is a model-independent measure of the spectral shape of the sources, it is not easy to interpret its evolution with source luminosity, as colour variations can be caused either by a variable normalization of the disc and Comptonization components, and/or by intrinsic variations of the hard band photon index. For this reason, Figs 2(b) and (e) show plots of the best-fitting X-ray photon

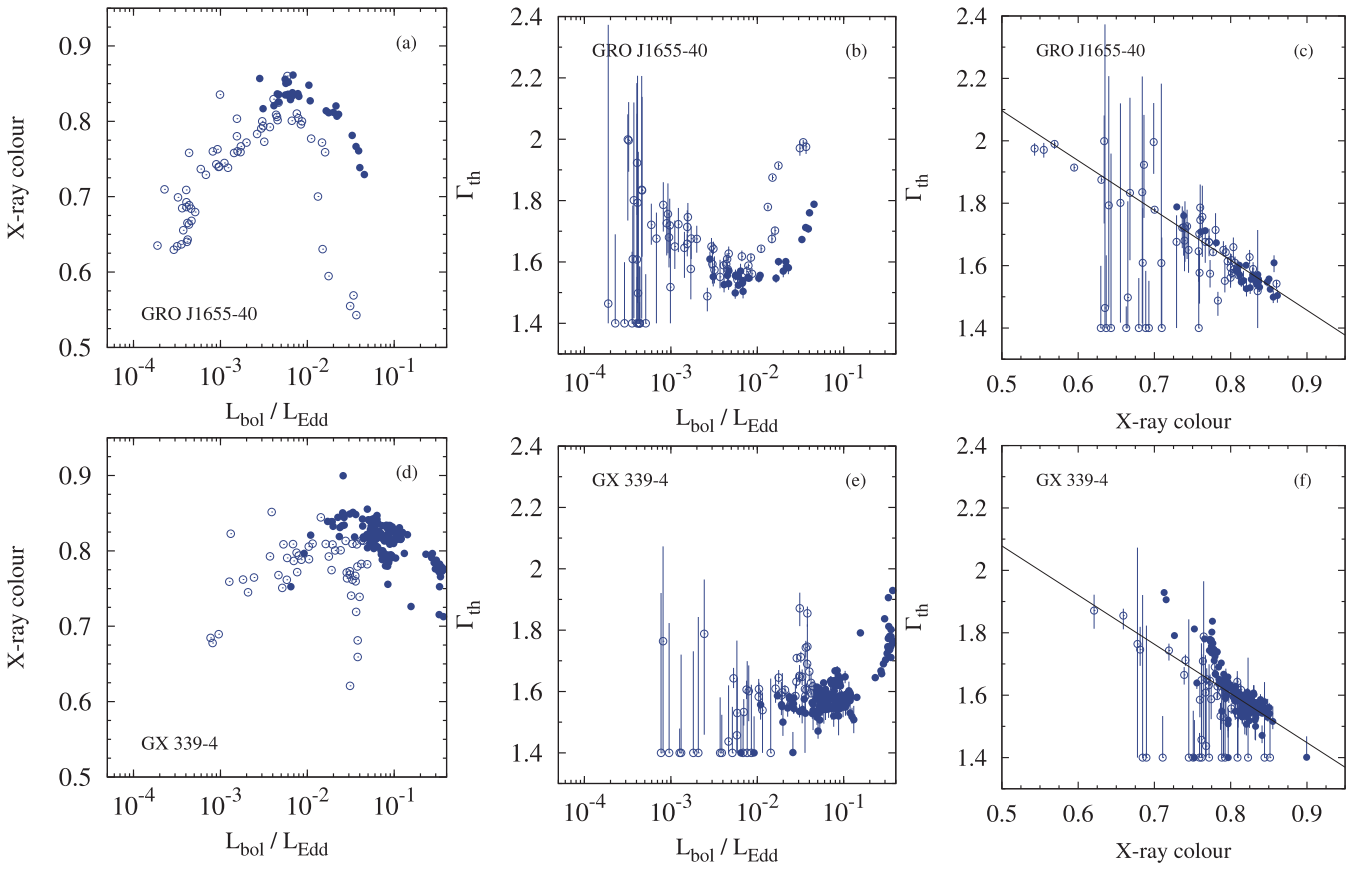

Figure 2. (a)/(d) The hard-state evolution of the X-ray colour with the luminosity in Eddington units in GRO J1655–40 and GX 339–4 (filled symbols, rising; open symbols, decaying). A hysteresis pattern can be seen in both sources. (b)/(e) The X-ray photon index as a function of the luminosity in Eddington units (the best-fitting photon indices are those reported by Sobolewska et al. 2009). (c)/(f) The correlation between the X-ray colour and the photon index, suggesting that in GRO J1655–40 and GX 339–4 the colour variations are caused by the photon index variations in the hard spectral state at all luminosity levels. The solid line represents the best-fitting linear function; for GX 339–4, we fit only the decay data (see text). The observations that give only upper limits on the photon index were neglected during the fit.

index from model 1 as a function of source luminosity, for the same observations that are plotted in Figs 2(a) and (d). The Γ values plotted in these panels correspond to the model 1 best-fitting results of Sobolewska et al. (2009).

The best-fitting Γ values for the lowest flux spectra have large errors associated with them. In fact, in some cases (especially GX 339–4), the best-fitting value reached the lowest boundary allowed during the fit, set to $\Gamma = 1.4$ (Sobolewska et al. 2009). In these cases, the photon index estimates should be considered as upper limits. These effects complicate the determination of the photon index evolution with luminosity, at the lowest flux states of the sources.

Overall, we believe that the evolution of Γ with $L_{\rm bol}/L_{\rm E}$, as shown in Figs 2(b) and (e), shows a pattern that is similar to that of X-ray colour evolution (Figs 2a and d). As the source luminosity increases, Γ becomes harder, until $L_{\rm bol}/L_{\rm E}$ reaches the level of a few per cent, above which the spectrum softens with increasing luminosity. This result suggests that, to a large extent, the X-ray colour evolution is caused by intrinsic photon index variations when GBHs are in their hard state. To strengthen this conclusion, we plot the photon index as a function of the X-ray colour in Figs 2(c) and (f). It is apparent that the two quantities correlate, and their dependence can be modelled with a linear function. During the fit, we neglect the data points that are upper limits (but we include these in Figs 2c and f), and we use the average of the upper and lower Γ errorbars (from model 1) as the error on Γ. We obtain $\Gamma_{\rm GRO} = (-1.60 \pm 0.04) \times C + (2.90 \pm 0.03)$ and $\Gamma_{\rm GX} = (-1.6 \pm 0.2) \times C + (2.9 \pm 0.2)$, where C denotes the X-ray colour. The fits result in relatively high χ^2/d.o.f. of 3.8 and 2.3 for GRO J1655–40 and GX 339–4, respectively. Nevertheless, it is clear that the model describes the observed anticorrelation well. In the case of GX 339–4, we fit only the data points of the outburst decay. The observations taken during the rising phase with $C > 0.8$ are consistent with the best fit. Those with the X-ray colour lower than $\sim$0.8 (and $L > 0.2L_{\rm E}$) seem to deviate from the best-fitting line. However, the photon index and colour anticorrelation also holds for these, with perhaps a different slope as a result of the relatively high luminosity of these hard-state spectra.

4.3 Correlation between $\ell_{\rm h}/\ell_{\rm s}$ and luminosity

Having fitted the hard-state spectra of the two sources with model 2, we can now investigate the observed spectral variations in a physically meaningful way, by studying variations of the hard-to-soft compactness ratio with luminosity. For typical coronal temperatures, the ratio of the hard-to-soft compactnesses determines the photon index of the hard X-ray continuum (e.g. Beloborodov 1999b). Consequently, under the hypothesis of inverse Compton produced X-rays, the observed spectral shape variations should be caused by the $\ell_{\rm h}/\ell_{\rm s}$ variations, which are associated mainly with the changes of the accretion geometry (e.g. the inner edge of the disc proceeding towards the black hole, or the presence of a coronal outflow with variable velocity).

We present the evolution of our best-fitting $\ell_{\rm h}/\ell_{\rm s}$ values as a function of luminosity in Figs 3 and 4. They clearly indicate that the observed decrease of the photon index and the increase of the X-ray colour with increasing luminosity up to a few per cent of the Eddington limit, are a result of the fact that $\ell_{\rm h}/\ell_{\rm s}$ increases from a value of $\sim$1 to $\sim$10–15 for the same range of $L_{\rm bol}/L_{\rm E}$, in both sources. At Eddington luminosity ratios higher than a few per cent, the $\ell_{\rm h}/\ell_{\rm s}$ evolution changes. It decreases with luminosity, leading to softer spectra (and lower values of X-ray colour).

In order to find the critical value of luminosity at which the compactness ratio reaches maximum, we fit a broken power-law model to the $\ell_{\rm h}/\ell_{\rm s}$ versus $L_{\rm bol}/L_{\rm E}$ data of the two sources. We summarize the fit results in Table 2. Similarly to the case of the photon index and X-ray colour correlation, we neglect measurements that are upper limits on $\ell_{\rm h}/\ell_{\rm s}$ (but we include these in the plots), and we use the average of the lower and upper $\ell_{\rm h}/\ell_{\rm s}$ errorbars (from model 2) as the error on $\ell_{\rm h}/\ell_{\rm s}$. In the case of GRO J1655–40, we fit the data from the rise and decay separately, and we calculate their weighted average, which gives $L_{\rm crit,GRO} = (0.0061 \pm 0.0002)L_{\rm E}$. In the case of GX 339–4, we treat each outburst separately, and we fit the rise and decay together for outbursts o1 and o3. We use only the decay data of outburst o2 because the data of the rise do not allow us to put meaningful constraints on the critical luminosity, and a strong hysteresis effect prevents a joint fitting of the rise and decay data. Again, we calculate the weighted average of the three measurements, and we obtain $L_{\rm crit,GX} = (0.011 \pm 0.002)L_{\rm E}$. During the fits we neglect several data points, indicated in Fig. 3 with light-grey symbols. These observations correspond to the periods shortly before/after the hard-to-soft/soft-to-hard spectral transition, when the compactness ratio, as well as the X-ray colour and photon index, change rapidly with luminosity.

However, the most significant contribution to the uncertainty on $L_{\rm crit}$ is introduced by the uncertainty of the GBH distance and mass

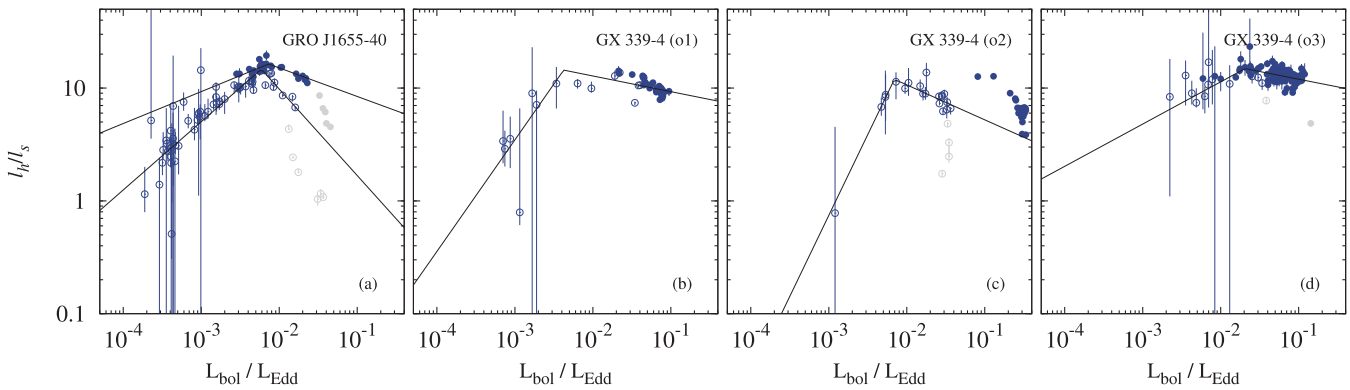

Figure 3. The hard-state heating-to-cooling compactness ratio of the corona, $\ell_{\rm h}/\ell_{\rm s}$, as a function of the luminosity in Eddington units for (a) GRO J1655–40 and (b)–(d) GX 339–4 (filled symbols, rising; open symbols, decaying). Solid lines indicate the broken power-law fits to the data. The light-grey data points were neglected during the fit (see Section 4.3). For GX 339–4, the best-fitting break luminosity is $L_{\rm crit,GRO} = (0.0061 \pm 0.0002)L_{\rm E}$, and the average of the fits to the three outbursts is $L_{\rm crit,GX} = (0.011 \pm 0.002)L_{\rm E}$.

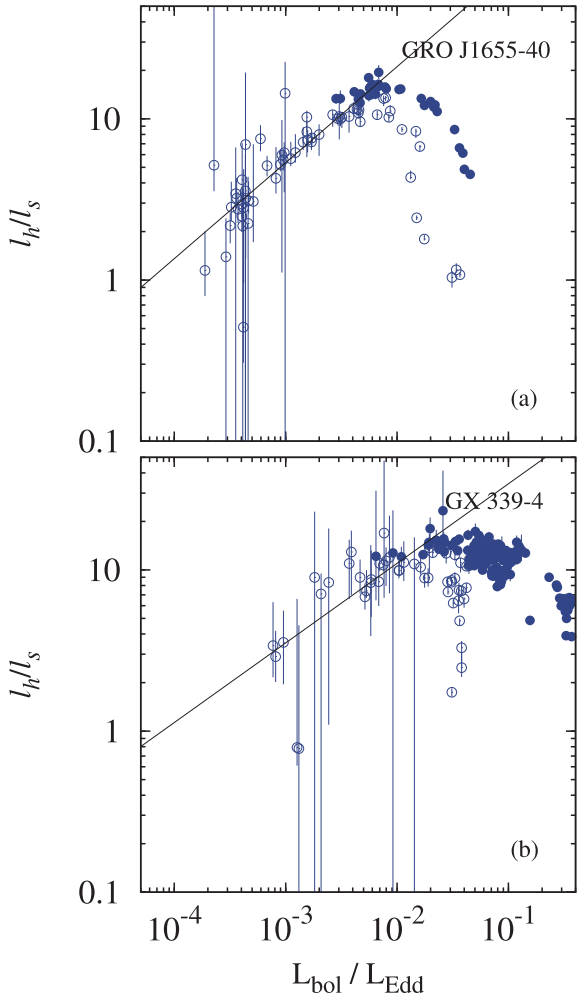

Figure 4. The hard-state heating-to-cooling ratio of the corona, ℓ_h/ℓ_s, as a function of the luminosity in Eddington units for (a) GRO J1655–40 and (b) GX 339–4 (filled symbols, rising; open symbols, decaying). Solid lines indicate the best-fitting model to the data with L_{bol} below L_{crit} (see Section 4.3). Best-fitting slopes are $a_{GRO} = 0.60 \pm 0.03$ and $a_{GX} = 0.49 \pm 0.15$.

Table 2. Coefficients in the ℓ_h/ℓ_s versus L_{bol}/L_E correlation.

Source	a	b	L_{crit}/L_E
GRO J1655–40	0.60 ± 0.03	328 ± 47	0.006
GX 339–4	0.49 ± 0.07	107 ± 39	0.01

estimates. Taking into account these uncertainties in the case of GX 339–4 (Table 1), we derive $0.003L_E < L_{crit,GX} < 0.04L_E$. In the case of GRO J1655–40, we obtain much tighter constraints: $0.005L_E < L_{crit,GRO} < 0.007L_E$. Foellmi (2009) derives an upper limit to GRO J1655–40, which differs substantially from the accepted value of 3.2 kpc. Adopting their upper limit of 2 kpc and $M = 6.3\,M_\odot$, we obtain $L_{crit,GRO} = 0.002L_E$. However, Caballero García et al. (2007) have pointed out that if GRO J1655–40 were indeed located so close, its companion star would not fill its Roche lobe. Given all the uncertainties, and the range of possible values for L_{crit} that we have presented, it seems quite possible that L_{crit}/L_E is the same in both objects, and roughly equal to ∼0.01.

Having determined the luminosity at which the evolution of ℓ_h/ℓ_s changes, we proceed to determining the slope of the ℓ_h/ℓ_s versus L_{bol}/L_E positive correlation below L_{crit}. We fitted jointly the rising and decaying data with luminosities below $L_{crit,GRO}$ and $L_{crit,GX}$, respectively, with the following function: $\ell_h/\ell_s = b \times (L_{bol}/L_E)^a$. The model describes well the anticorrelation between ℓ_h/ℓ_s and luminosity (χ^2/d.o.f. equals 1.5 and 0.7 for GRO J1655–40 and GX 339–4, respectively). The solid lines in Figs 4(a) and (b) indicate the best-fitting models. The best-fitting values are $a_{GRO} = 0.60 \pm 0.03$, $a_{GX} = 0.49 \pm 0.07$, $b_{GRO} = 328 \pm 47$ and $b_{GX} = 107 \pm 39$ (Table 2). These are consistent within their errors for the two sources, and their weighted means are $\bar{a} = 0.58 \pm 0.02$ and $\bar{b} = 197 \pm 30$.

4.4 Quiescence

The anticorrelation between ℓ_h/ℓ_s and the Eddington luminosity ratio does not extend to the quiescence. This conclusion is based on the Eddington luminosity ratios and photon indices collected for quiescent accreting GBHs by Corbel, Tomsick & Kaaret (2006): XTE J1118+480, A0620–00, XTE J1550–564, GX 339–4, GRO J1655–40 and V641 Sgr. We have also included three measurements for V404 Cyg. In two cases, we combined the reported photon indices with the Eddington luminosity ratios calculated based on the 0.3–10 keV *XMM–Newton* unabsorbed flux (Bradley et al. 2007) and the 3–9 keV *Chandra* flux (Corbel, Koerding & Kaaret 2008), assuming $M = 12\,M_\odot$ and $D = 3.5$ kpc (Corbel et al. 2006). The third quiescent observation of V404 Cyg was originally published by Kong et al. (2002). However, it was claimed to be affected by pile-up, so we adopted the pile-up corrected photon index of Corbel et al. (2008), and the Eddington luminosity ratio as in Kong et al. (2002).

These quiescent measurements of the photon index are consistent with being constant, $\Gamma_q = 2.13 \pm 0.06$, as a function of luminosity. In Fig. 5, we again plot the hard-state data of GRO J1655–40 and GX 339–4, together with ℓ_h/ℓ_s calculated based on the quiescent photon indices using the following equation, $\Gamma = 2.33 \times (\ell_h/\ell_s)^{-1/6}$

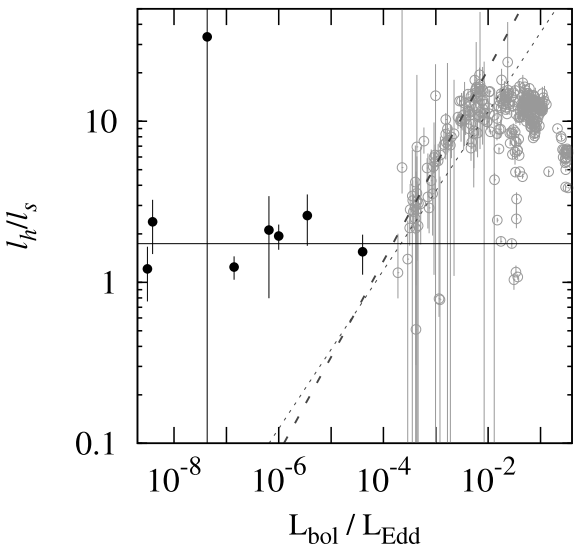

Figure 5. Comparison of the hard state and quiescent state. Data and fits to GRO J1655–40 and GX 339–4 are as in Fig. 4 (open/grey symbols, dashed and dotted lines, respectively). The filled/black symbols represent the measurements for several GBHs collected from the literature (see Section 5.5). In quiescence, the ℓ_h/ℓ_s saturates at ∼1.7 (solid horizontal line).

(Beloborodov 1999b). We conclude that, in quiescence, the heating-to-cooling compactness ratio saturates at $\ell_h/\ell_s \sim 1.7$, corresponding to Γ_q.

5 DISCUSSION

We have studied two confirmed GBHs, GX 339–4 and GRO J1655–40, considering all their archival *RXTE* observations until 2007 June. We have focused on a subset of observations, when the photon index was smaller than 2 (i.e. when the sources were mainly in the hard state). During these observations, the source luminosity was lower than 10 per cent of the Eddington limit in the case of GRO J1655–40, and 30 per cent in GX 339–4.

We have used traditional X-ray colours and the results of Sobolewska et al. (2009) to determine the spectral evolution of each source. Our results are consistent with what has been observed in the past, for other GBHs and active galactic nuclei as well: the X-ray colour increases and the photon index hardens, with increasing luminosity, up to the point where $L_{bol}/L_E \sim 0.01$. Above this point, the opposite trend is observed: a decrease of the X-ray colour and a softening of the photon index with increasing luminosity.

Within the context of thermal Comptonization models for the X-ray production in accreting black holes, the photon index is determined by the hard-to-soft compactness ratio, ℓ_h/ℓ_s. The main result of our work is that the observed spectral variations of the two sources, when in the hard state, can be explained if ℓ_h/ℓ_s and luminosity are anticorrelated for luminosities below $L_{crit} \sim 0.01 L_E$, and positively correlated for luminosities higher than L_{crit}. The anticorrelation below L_{crit} can be described by $\ell_h/\ell_s \propto L_{bol}^{\bar{a}}$, where $\bar{a} = 0.58 \pm 0.02$ is the weighted mean for both objects.

Because the compactness ratio, ℓ_h/ℓ_s, depends mainly on the geometry of the accretion flow, our results can put constraints on various models that have been proposed to explain the hard X-ray emission in GBHs. In the following, we discuss some of these constraints and the implications of our results. We note that in the hard-state spectra of GBHs the Comptonized emission dominates over the emission of the seed photons, so that $L_{bol} \propto \ell_h$.

5.1 Hot thermal inner flow, truncated disc seeds

The hard X-rays could be produced by Compton upscattering of seed photons from a disc illuminating a hot inner flow. Heat conduction from thermal contact of the hot flow and cool disc can lead to evaporation of the inner thin disc, resulting in a truncated thin disc, with a radius of $R_{disc} \propto \dot{m}^{-1/2}$ (Czerny, Rózańska & Kuraszkiewicz 2004). We assume that the hot flow is powered by the same mass accretion rate that flows through the thin disc, so that its luminosity is given by the remaining potential energy from the inner edge of the truncated disc, R_{disc}, to the inner edge of the hot flow, R_{in}. Then (approximately)

$$\ell_h \sim GM\dot{m}(1/R_{in} - 1/R_{disc}) \times \eta_{corona}/\eta_{disc},$$

where $\eta_{corona}/\eta_{disc}$ is the radiative efficiency of the hot flow relative to that of a thin disc, and it is proportional to $\dot{m}$ for a radiatively inefficient flow (e.g. Sharma et al. 2007), and roughly constant for a radiatively efficient flow. If we assume that $R_{disc} \gg R_{in}$, then $\ell_h \propto \dot{m}\eta_{corona}/\eta_{disc}$, which implies that $\ell_h \propto \dot{m}^2$ for a radiatively inefficient flow and $\ell_h \propto \dot{m}$ for a radiatively efficient flow. The truncated disc luminosity is $L_{disc} = GM\dot{m}_{disc}/2R_{disc}$, but only part of this is intercepted by the hot Comptonization region, which we assume to be a sphere of radius R_h. This fraction, f, varies with radius, and it reaches maximum at the truncation radius of the disc, where $f = (R_h/R_{disc})^2/\pi$. Because the disc luminosity peaks at the same radius, the seed photon luminosity for the hot flow is

$$\ell_s \approx GM\dot{m}/2R_{disc} \times (R_h/R_{disc})^2/\pi,$$

so that

$$\ell_h/\ell_s = 2\pi \times (R_{disc}/R_{in}) \times (R_{disc}/R_h)^2 \times \eta_{corona}/\eta_{disc}.$$

We obtain $\ell_h/\ell_s \propto \dot{m}^{-3/2}\eta_{corona}/\eta_{disc} \propto \ell_h^{-1/4}$ for a radiatively inefficient flow, and proportional to $\ell_h^{-3/2}$ for a radiatively efficient flow. Either way, this predicts that ℓ_h/ℓ_s increases as the luminosity decreases (i.e. that the spectrum hardens at lower luminosities). This is mainly because of the rapidly decreasing solid angle subtended by the hot flow to the truncated disc. However, this is in marked contrast to the observed softening of the spectrum seen at the lowest luminosities, followed by the saturation in quiescence, ruling out this scenario as the physical mechanism for the observed X-ray emission at luminosities below L_{crit}.

However, this could instead explain the observed behaviour above L_{crit}, where the spectrum abruptly softens with increasing luminosity. Hence, there must be a transition to another mechanism at L_{crit} to explain the change in the behaviour of ℓ_h/ℓ_s.

5.2 Hot thermal inner flow, cyclo-synchrotron seeds

There are also seed photons generated in the hot flow itself, by cyclo-synchroton radiation of the energetic electrons. This emission is strongly self-absorbed for thermal electrons, so it peaks at the self-absorption frequency ν_{ssa}, given where the cyclo-synchrotron emissivity equals that of a blackbody. The full equation for this is complex (Narayan & Yi 1995). However, Wardziński & Zdziarski (2000) give a numerical approximation for this frequency, $\nu_{ssa} \propto \theta^{0.95}\tau^{0.05}B^{0.91}$, where θ and τ are the dimensionless temperature and optical depth of the electrons in the hot flow, respectively, and B is the magnetic field. At the observed temperatures, ν_{ssa} should be on the Rayleigh–Jeans tail of the blackbody, so the flux at this point is $\propto \nu_{ssa}^2\theta$. Thus, the seed photon luminosity $\ell_s \propto \nu_{ssa}^3\theta$. The hard luminosity is as before, with $\ell_h = GM\dot{m}/2R_{in} \times \eta_{corona}/\eta_{disc}$, and hence $\ell_h/\ell_s \propto \ell_h/(\theta^{3.85}\tau^{0.15}B^{2.73})$.

We obtain a further constraint as ℓ_h/ℓ_s is also set by θ and τ. Pietrini & Krolik (1995) give an approximation for this of $0.1(\ell_h/\ell_s)^{1/4} = \theta\tau$. This gives $\ell_h/\ell_s \propto \ell_h^{0.51}\tau^{1.19}(\tau/B^2)^{0.70}$. In a radiatively inefficient flow, the gas pressure is set by the ion temperature, which remains approximately constant around the virial temperature. Hence, τ/B^2 is constant if the magnetic pressure is a constant fraction of the gas pressure. Hence, $\ell_h/\ell_s \propto \ell_h^{0.51}\tau^{1.19} \propto \ell_h^{1.1}$ if $\tau \propto \dot{m} \propto \ell_h^{1/2}$. This is faster than the observed $\ell_h/\ell_s \propto \ell_h^{0.5-0.6}$, but given the level of approximation this at least describes the observed trend below L_{crit} for the spectrum to soften as the luminosity decreases.

However, this alone does not give a framework for the change in behaviour at higher luminosities, where the spectrum dramatically softens with increasing luminosity. Thus, neither seed photons from the disc nor self-produced synchrotron self-Compton photons from the flow can explain the full range of observed behaviour, although the combination of the two (seed photons from the disc changing to seed photons from cyclo-synchrotron as luminosity decreases) can explain the observations.

The saturation observed in quiescence is not expected if the electron distribution in the hot flow is thermal. However, it is likely that the electron distribution is not purely Maxwellian. Evidence for the presence of a non-thermal high-energy tail in the electron

distribution has been found in the hard state of several black hole binaries (McConnell et al. 2002; Wardziński et al. 2002; Cadolle Bel et al. 2006; Joinet et al. 2007; Droulans et al. 2010). Consequently, in quiescence, while the plasma becomes optically thin (because of decreasing $L/L_{\rm E}$), the Comptonized component becomes dominated by the contribution arising through scattering on the non-thermal high-energy electrons, and the evolution of Γ (and hence $\ell_{\rm h}/\ell_{\rm s}$) depends on the microphysics of particle acceleration in the corona. Particle acceleration with a slope that does not depend on $L/L_{\rm E}$ would result in a saturation of $\ell_{\rm h}/\ell_{\rm s}$.

5.3 Outflowing hot thermal corona, untruncated disc

An outflowing hot corona above an untruncated disc is an alternative geometry to explain the observed hard spectra seen in the hard state (Beloborodov 1999a; Malzac et al. 2001). Here, the seed photons for Compton scattering are from the disc, but are suppressed by relativistic beaming from the mildly outflowing corona.

In the original model of Beloborodov (1999a), the intrinsic disc emission is assumed to be negligible compared to reprocessed radiation produced by the disc illumination by the X-ray source. Then, $\ell_{\rm h}/\ell_{\rm s}$ depends mainly on the outflow velocity (as well as a few geometric parameters). As the velocity increases, beaming reduces the illumination of the disc and the soft photon flux returns to the outflow. Therefore, as the velocity increases, the ratio $\ell_{\rm h}/\ell_{\rm s}$ increases, and the reflected fraction decreases. We also note that in the outflowing corona model, the luminosity of the corona is amplified by relativistic beaming. This affects the shape of the observed correlations between $\ell_{\rm h}/\ell_s$ and luminosity.

The observed spectral softening (and correlated increase in reflected fraction; e.g. Gilfanov, Churazov & Revnivtsev 1999; Ibragimov et al. 2005) seen above $L_{\rm crit}$ can be explained in this model if the outflow velocity (and hence $\ell_{\rm h}/\ell_{\rm s}$) decreases as luminosity increases. The change in behaviour below $L_{\rm crit}$ then requires that the outflow velocity decreases as luminosity decreases. This makes a clear prediction that at the lowest luminosities where the beaming is negligible, the continuum should be accompanied by a substantial reflected emission from an untruncated disc and ℓ_h/ℓ_s should saturate, as observed.

Alternatively, the softening of the spectrum below $L_{\rm crit}$ could also be caused by an increase in intrinsic emission from the disc such that this dominates over the reprocessed emission as the source of seed photons. The outflow velocity could then remain high, or even continue to increase as luminosity decreases. This predicts that the reflected fraction remains small, but that the observed fraction of power dissipated in the disc should increase.

5.4 Non-thermal jet, untruncated disc

Another type of emission suggested to explain the hard X-ray spectrum is direct non-thermal synchrotron radiation from a jet (Markoff, Nowak & Wilms 2005). Both thermal Comptonization and jet models can reproduce the shape and observed energy range of the spectral cut-offs seen in the hard states (e.g. Zdziarski et al. 2003; Markoff & Nowak 2004). In several black hole binaries, the cut-off energy was reported to anticorrelate with luminosity in a bright hard state (e.g. Wardziński et al. 2002; Rodriguez et al. 2003; Miyakawa et al. 2008; Joinet et al. 2008; Motta et al. 2009). This can be explained naturally in terms of thermal Comptonization models by enhanced cooling by the disc photons. Thus, it seems likely that thermal Comptonization does dominate at $L_{\rm bol}/L_{\rm E} > 0.01$. It is then possible that the transition in spectral behaviour seen at $L_{\rm crit}$ marks the point at which non-thermal emission from the jet starts to dominate over thermal Comptonization from the hot flow (Russell et al. 2010). Theoretical models of jet-dominated accretion flows (e.g. Falcke & Markoff 2000; Markoff, Falcke & Fender 2001; Yuan, Markoff & Falcke 2002) certainly predict that the kinetic power of the jet exceeds the radiative luminosity (see also Malzac, Merloni & Fabian 2004; Malzac, Belmont & Fabian 2009). However, the photon index of the X-ray emission then depends on the photon index of the non-thermal electrons within the jet. So, in order to explain the spectral softening with decreasing luminosity it is necessary for the electron heating/cooling processes to result in a steeper electron distribution. There are currently no real constraints on this, because of the lack of knowledge of jet physics.

In quiescence, similar to the case of non-thermal Comptonization dominating the X-ray in the scenario involving thermal inner flow and cyclo-synchrotron seeds, the saturation of $\ell_{\rm h}/\ell_{\rm s}$ can be explained in the jet model if the slope of accelerated non-thermal particles in the jet is independent of $L/L_{\rm E}$.

6 CONCLUSIONS

We show that in the hard state of GBHs the compactness ratio $\ell_{\rm h}/\ell_{\rm s}$ reaches maximum at $L_{\rm crit} \sim 0.01 L_{\rm E}$. For $L_{\rm bol} < L_{\rm crit}$, we find that $\ell_{\rm h}/\ell_{\rm s} = \bar{b} \times (L_{\rm bol}/L_{\rm E})^{\bar{a}}$, where $\bar{a} = 0.58 \pm 0.02$ and $\bar{b} = 197 \pm 30$ are the weighted slope and intercept, respectively, based on the fits to the data of GRO J1655–40 and GX 339–4. We suggest that the change of behaviour in the $\ell_{\rm h}/\ell_{\rm s}$ versus luminosity relation is caused by a change in the X-ray emission mechanism for the hard-state spectra of GBHs. The relation does not extend to the quiescent state. Instead, a saturation of $\ell_{\rm h}/\ell_{\rm s}$ is observed at a value of $\sim$1.7.

The observed hard-state evolution of $\ell_{\rm h}/\ell_{\rm s}$ can be explained if the seed photons are cyclo-synchrotron photons up to $L_{\rm crit}$, above which they are replaced with the truncated disc photons. Alternatively, the observed variability of $\ell_{\rm h}/\ell_{\rm s}$ can be explained in the case of an outflowing corona, if the outflow velocity increases with luminosity up to $L_{\rm crit}$ and then decreases with increasing luminosity, or if the seed intrinsic disc photons are replaced with the reprocessed photons above $L_{\rm crit}$. Finally, in the scenario involving an X-ray emitting jet, the observed transition in the behaviour of $\ell_{\rm h}/\ell_{\rm s}$ might mark the point at which the non-thermal jet emission starts dominating over the thermal Comptonization emission.

Observed saturation of $\ell_{\rm h}/\ell_{\rm s}$ in quiescence can be explained in terms of an untruncated disc model with cyclo-synchrotron seed (and in the jet model) if the non-thermal particles in the corona (jet) are accelerated with a slope that is independent of $L/L_{\rm E}$. The outflowing corona model naturally predicts the quiescent saturation of $\ell_{\rm h}/\ell_{\rm s}$ if the outflow velocity decreases with luminosity below $L_{\rm crit}$.

ACKNOWLEDGMENTS

We would like to thank the anonymous referee for helpful comments and suggestions. MS acknowledges support from a *Chandra* grant GO8-9125A and a Marie-Curie ToK Fellowship number MTKD-CT-2006-039965. IEP acknowledges support from the EU FP7-REGPOT 206469 grant. This work was partially supported by the GdR PCHE in France.

REFERENCES

Arnaud K. A., 1996, Astronomical Data Analysis Software and Systems V, 101, 17

Belloni T., Homan J., Casella P., van der Klis M., Nespoli E., Lewin W. H. G., Miller J. M., Méndez M., 2005, A&A, 440, 207
Beloborodov A. M., 1999a, ApJ, 510, L123
Beloborodov A. M., 1999b, in Poutanen J., Svensson R., eds, ASP Conf. Ser. Vol. 161, High-Energy Processes in Accreting Black Holes. Astron. Soc. Pac., San Francisco, p. 295
Bradley C. K., Hynes R. I., Kong A. K. H., Haswell C. A., Casares J., Gallo E., 2007, ApJ, 667, 427
Caballero García M. D. et al., 2007, ApJ, 669, 534
Cadolle Bel M. et al., 2006, A&A, 446, 591
Constantin A., Green P., Aldcroft T., Kim D. W., Haggard D., Barkhouse W., Anderson S. F., 2009, ApJ, 705, 1336
Coppi P. S., 1999, in Poutanen J., Svensson R., eds, ASP Conf. Ser. Vol, 161, High-Energy Processes in Accreting Black Holes. Astron. Soc. Pac., San Francisco, p. 375
Corbel S., Fender R. P., Tomsick J. A., Tzioumis A. K., Tingay S., 2004, ApJ, 617, 1272
Corbel S., Tomsick J. A., Kaaret P., 2006, ApJ, 636, 971
Corbel S., Koerding E., Kaaret P., 2008, MNRAS, 389, 1697
Czerny B., Rózańska A., Kuraszkiewicz J., 2004, A&A, 428, 39
Done C., Gierliński M., 2003, MNRAS, 342, 1041
Done C., Gierliński M., Kubota A., 2007, A&AR, 15, 1
Droulans R., Belmont R., Malzac J., Jourdain E., 2010, ApJ, 717, 1022
Dunn R. J. H., Fender R. P., Körding E. G., Cabanac C., Belloni T., 2008, MNRAS, 387, 545
Dunn R. J. H., Fender R. P., Körding E. G., Belloni T., Cabanac C., 2010, MNRAS, 403, 61
Ebisawa K. et al., 1994, PASJ, 46, 375
Esin A. A., McClintock J. E., Narayan R., 1997, ApJ, 489, 865
Falcke H., Markoff S., 2000, A&A, 362, 113
Fender R. P., Belloni T. M., Gallo E., 2004, MNRAS, 355, 1105
Foellmi C., 2009, Nat, 14, 674
Gierliński M., Newton J., 2006, MNRAS, 370, 837
Gierliński M., Zdziarski A. A., Poutanen J., Coppi P. S., Ebisawa K., Johnson W. N., 1999, MNRAS, 309, 496
Gilfanov M., Churazov E., Revnivtsev M., 1999, A&A, 352, 182
Gladstone J., Done C., Gierliński M., 2007, MNRAS, 378, 13
Gu M., Cao X., 2009, MNRAS, 399, 349
Hynes R. I., Steeghs D., Casares J., Charles P. A., O'Brien K., 2004, ApJ, 609, 317
Ibragimov A., Poutanen J., Gilfanov M., Zdziarski A. A., Shrader C. R., 2005, MNRAS, 362, 1435
Joinet A., Jourdain E., Malzac J., Roques J. P., Corbel S., Rodriguez J., Kalemci E., 2007, ApJ, 657, 400
Joinet A., Kalemci E., Senziani F., 2008, ApJ, 679, 655
Jonker P. G., Gallo E., Dhawan V., Rupen M., Fender R. P., Dubus G., 2004, MNRAS, 351, 1359
Kalemci E., Tomsick J. A., Buxton M. M., Rothschild R. E., Pottschmidt K., Corbel S., Brocksopp C., Kaaret P., 2005, ApJ, 622, 508
Kolehmainen M., Done C., 2010, MNRAS, 406, 2206
Kong A. K. H., McClintock J. E., Garcia M. R., Murray S. S., Barret D., 2002, ApJ, 570, 277
Laor A., 1991, ApJ, 376, 90
McConnell M. L. et al., 2002, ApJ, 572, 984
Malzac J., Beloborodov A. M., Poutanen J., 2001, MNRAS, 326, 417
Malzac J., Merloni A., Fabian A. C., 2004, MNRAS, 351, 253
Malzac J., Belmont R., Fabian A. C., 2009, MNRAS, 400, 1512
Markoff S., Nowak M. A., 2004, ApJ, 609, 972
Markoff S., Falcke H., Fender R., 2001, A&A, 372, L25
Markoff S., Nowak M. A., Wilms J., 2005, ApJ, 635, 1203
Meyer-Hofmeister E., Liu B. F., Meyer F., 2005, A&A, 432, 181
Meyer-Hofmeister E., Liu B. F., Meyer F., 2009, A&A, 508, 329
Miyakawa T., Yamaoka K., Homan J., Saito K., Dotani T., Yoshida A., Inoue H., 2008, PASJ, 60, 637
Motta S., Belloni T., Homan J., 2009, MNRAS, 400, 1603
Muñoz-Darias T., Casares J., Martínez-Pais I. G., 2008, MNRAS, 385, 2205
Narayan R., Yi I., 1995, ApJ, 452, 710
Orosz J. A., Bailyn C. D., 1997, ApJ, 477, 876
Pietrini P., Krolik J. H., 1995, ApJ, 447, 526
Porquet D., Reeves J. N., O'Brien P., Brinkmann W., 2004, A&A, 422, 85
Remillard R. A., McClintock J. E., 2006, ARA&A, 44, 49
Revnivtsev M. G., Trudolyubov S. P., Borozdin K. N., 2000, MNRAS, 312, 151
Rodriguez J., Corbel S., Tomsick J. A., 2003, ApJ, 595, 1032
Russell D. M., Maitra D., Dunn R. J. H., Markoff S., 2010, MNRAS, 405, 1759
Saez C., Chartas G., Brandt W. N., Lehmer B. D., Bauer F. E., Dai X., Garmire G. P., 2008, AJ, 135, 1505
Sharma P., Quataert E., Hammett G. W., Stone J. M., 2007, ApJ, 667, 714
Shemmer O., Brandt W. N., Netzer H., Maiolino R., Kaspi S., 2006, ApJ, 646, L29
Sobolewska M. A., Papadakis I. E., 2009, MNRAS, 399, 1597
Sobolewska M. A., Gierliński M., Siemiginowska A., 2009, MNRAS, 394, 1640
Sobolewska M. A., Siemiginowska A., Gierliński M., 2011, MNRAS, 413, 2259
Wardziński G., Zdziarski A. A., 2000, MNRAS, 314, 183
Wardziński G., Zdziarski A. A., Gierliński M., Grove J. E., Jahoda K., Johnson W. N., 2002, MNRAS, 337, 829
Wu Q., Gu M., 2008, ApJ, 682, 212
Yuan F., Markoff S., Falcke H., 2002, A&A, 383, 854
Zdziarski A. A., Johnson W. N., Magdziarz P., 1996, MNRAS, 283, 193
Zdziarski A. A., Lubiński P., Gilfanov M., Revnivtsev M., 2003, MNRAS, 342, 355
Zdziarski A. A., Gierliński M., Mikołajewska J., Wardziński G., Smith D. M., Harmon B. A., Kitamoto S., 2004, MNRAS, 351, 791

This paper has been typeset from a TEX/LATEX file prepared by the author.